

# Generalized sine-Gordon solitons

C. dos Santos<sup>1</sup>, D. Rubiera-Garcia<sup>2</sup>

<sup>1</sup>*Centro de Física e Departamento de Física e Astronomia,  
Faculdade de Ciências da Universidade do Porto, 4169-007 Porto, Portugal.*

<sup>2</sup>*Departamento de Física, Universidad de Oviedo,  
Avenida Calvo Sotelo 18, 33007 Oviedo, Asturias, Spain.*

(Dated: July 27, 2011)

In this paper we construct analytical self-dual soliton solutions in (1+1) dimensions for two families of models which can be seen as generalizations of the sine-Gordon system but where the kinetic term is non-canonical. For that purpose we use a projection method applied to the Sine-Gordon soliton. We focus our attention on the wall and lump-like soliton solutions of these k-field models. These solutions and their potentials reduce to those of the Klein-Gordon kink and the standard lump for the case of canonical kinetic term. As we increase the non-linearity on the kinetic term the corresponding potentials get modified and the nature of the soliton may change, in particular, undergoing a topology modification. The procedure constructed here is shown to be a sort of generalization of the deformation method for a specific class of k-field models.

PACS numbers: 03.50.-z, 05.45.Yv, 11.27.+d

## I. INTRODUCTION

K-fields are field theories where the kinetic term is non-canonical and whose soliton solutions have been intensively studied due to their applications in strong interaction physics [1], topological defects [2, 3] and cosmology [4] with the result that their properties can be quite different from the standard canonical ones. For example these solitons can have a compact support [5].

The aim of this paper is to present a method to construct *analytical* soliton solutions in (1+1) dimensions in k-field theories and relate it with the deformation method developed by Bazeia et al. and originally introduced in Ref.[6]. Such soliton solutions may be of wall or lump-like type. We take the context of the sine-Gordon model [7], as one of the most interesting solitons in integrable (1 + 1) dimensional systems.

The deformation method, used in a wide range of contexts, has also been employed in the sine-Gordon one and its modifications where the scalar potential  $V(\phi)$  is given by polynomial interactions obtained from truncations of the sine-Gordon one [8] allowing then to get new families of sine-Gordon models [9].

Sine-Gordon solitons have physically attractive properties, as they can be used to describe many physical phenomena, such as the Josephson junctions [10] and systems with one-dimensional dislocations [11], but also mathematical ones such as the description of spaces with constant negative curvature [12] or simply being objects of interest by their own on integrable and conformal field theories [13].

Moreover solitons are of current interest due to its applications to supergravity [14], brane cosmology [15], but also to other areas of nonlinear science [16], in particular in the study of macromolecules such as the DNA [17].

In several of the above areas the deformation method has been shown to be a useful tool for the analysis of diverse problems. The method developed in this paper

extends that one to a class of k-fields defined as powers of the canonical kinetic term, using as the starting point the sine-Gordon model. This kind of choice in the kinetic term for electromagnetic fields has been considered in Ref.[18]. By doing this we shall obtain several families of k-field models with kink and lump-like solutions, which are of current interest to high-energy physics; for example, in the context of their embedding in higher dimensions as they may play a role in the braneworld context [19], and as cosmological domain walls [20].

This paper is organized as follows: in Sec II we briefly review the sine-Gordon model and its cosine-Gordon counterpart. In Sec. III we present the generic formalism for k-field theories and discuss the necessary conditions to have self-dual solutions. In Sec. IV we present several examples of k-field models, obtain analytical soliton solutions and study their physical properties. In Sec. V we compare our results with those obtained by using the deformation method and we conclude in section VI by drawing some conclusions and future perspectives.

## II. SINE-GORDON SYSTEM

This section is divided into two parts: in the first one we briefly review static soliton solutions in (1+1) dimensions for the sine-Gordon model [7]. In the second part we employ the same procedure but now for analysis of the cosine-Gordon model.

### A. Sine-Gordon model

The (1+1)-dimensional lagrangian density for the sine-Gordon model [7] is given by

$$L = \frac{1}{2} \partial_\mu \phi \partial^\mu \phi - \frac{\alpha}{\beta^2} (1 - \cos[\beta \phi]), \quad (1)$$

where  $\phi$  is a single real scalar field and  $\alpha$  and  $\beta$  are two positive parameters. By convenience we take  $\alpha = 1$  and  $\beta = 2$  which brings that the scalar potential writes

$$V(\phi) = \frac{1}{2} \sin^2[\phi]. \quad (2)$$

For further reference we also write

$$X = \frac{1}{2} \partial_\mu \phi \partial^\mu \phi, \quad (3)$$

for the standard canonical kinetic term.

For static fields the Euler Lagrange equations of motion are

$$\phi'' = \frac{1}{2} \sin[2\phi], \quad (4)$$

which for the Bogomon'nyi-Prasad-Sommerfeld (BPS) states [21] becomes of first order and is given by the relation

$$\phi' = \sin[\phi]. \quad (5)$$

The kink solution is well known [22] and is given by

$$\phi_0(x) = 2 \arctan[e^{(x-x_0)}], \quad (6)$$

which is located at  $x = x_0$  and satisfies the boundary conditions  $\phi(x = -\infty) = 0$  and  $\phi(x = +\infty) = \pi$ .

Let us note that the standard Klein-Gordon kink solution, i.e., the soliton solution for the standard Higgs potential  $\frac{1}{2}(1 - \phi^2)^2$ , which is given by  $\tanh[x - x_0]$  may be written in terms of the sine-Gordon solution,  $\phi_0$ , as

$$\phi_1 = -\cos[\phi_0]. \quad (7)$$

This means that the standard kink soliton solution may be seen as a projection of the field  $\phi_0$  (which thus can be seen as an “angle”) over the real axis.

In the same way the standard lump, soliton solution of the potential  $\frac{1}{2}(1 - \phi^2)\phi^2$ , which is given by  $\cosh[x - x_0]^{-1}$ , can be seen as a projection of the sine-Gordon field  $\phi_0$  but now over the imaginary axis

$$\phi_2 = \sin[\phi_0]. \quad (8)$$

We now note that the sine-Gordon potential, i.e.,

$$V(\phi) = \frac{\alpha}{\beta^2} (1 - \cos[\beta\phi]), \quad (9)$$

has a infinite number of vacua given by the solutions  $\phi_0 = 2\pi n/\beta$ . Consequently the lagrangian (1) with this potential is invariant under shifts of the field of the form  $\phi_0 \rightarrow \phi_0 + 2\pi n/\beta$  leading to different topological sectors labeled by the charge  $Q = \frac{\beta}{2\pi}(\phi_0(+\infty) - \phi_0(-\infty))$ .

Let us stress that besides the static kink soliton solution, the sine-Gordon model also admits anti-kink, breather, wobbles and kink-breather solutions [23].

## B. Cosine-Gordon model

Let us now perform a field shift in the potential given in (2) to take

$$\bar{\phi} = \phi - \frac{\pi}{2}, \quad (10)$$

bringing that the potential now becomes

$$\bar{V}(\bar{\phi}) = \frac{1}{2} \cos^2[\bar{\phi}], \quad (11)$$

which shall be called, by convenience, the “cosine-Gordon” model. Its static BPS kink is given by

$$\bar{\phi}_0(x) = 2 \arctan[\tanh[\frac{x - \bar{x}_0}{2}]], \quad (12)$$

which is the solution of the first order equation of motion

$$\bar{\phi}' = \cos[\bar{\phi}], \quad (13)$$

with the boundary conditions  $\bar{\phi}(x = -\infty) = -\frac{\pi}{2}$  and  $\bar{\phi}(x = +\infty) = \frac{\pi}{2}$ .

One gets that now, when applying the “projection” method underlined above, the standard Klein-Gordon kink and the lump soliton solution considered above, i.e.,  $\phi_W$  and  $\phi_L$  are, respectively, given by

$$\phi_W = \sin(\bar{\phi}); \phi_L = \cos(\bar{\phi}). \quad (14)$$

The reason to consider this “cosine-Gordon” model, as shall become clear later, is the fact that the projected models constructed on Sec. IV, i.e., models of family A and B, *do not retain the original symmetry of the sine-Gordon model*. Therefore, the projections applied to the sine-Gordon or to the cosine-Gordon model will be, in general, different, as shall be seen at once.

## III. GENERIC FORMALISM FOR K-FIELD MODELS

Let us now introduce the generic formalism for k-field models with non-canonical kinetic term  $F(X)$  and potential  $V(\phi)$  in  $(1 + 1)$  dimensions. Its action is given by

$$S = \int d^2x L = \int d^2x (F(X) - V(\phi)), \quad (15)$$

where  $F(X)$  is an arbitrary function of the D’Alambert lagrangian defined in Eq.(3). The associated energy-momentum tensor is obtained as

$$T^{\mu\nu} = F_X \partial^\mu \phi \partial^\nu \phi - \eta^{\mu\nu} L. \quad (16)$$

From now on we shall only consider static configurations  $\phi = \phi(x)$ , for which the non-vanishing components of the

energy-momentum tensor are given by (we are defining  $F_X \equiv \frac{dF}{dX}$ )

$$\begin{aligned} T^{00} &= \varepsilon = -L = -F(X) + V(\phi) \\ T^{11} &= -p = F(X) - 2XF_X, \end{aligned} \quad (17)$$

where  $\varepsilon$  and  $p$  are the energy density and the pressure, respectively. Note that the positive definiteness of the energy density implies  $F_X > 0$ .

The equations of motion for the action (15) are obtained as

$$\partial_\mu(F_X \partial^\mu \phi) + \frac{\partial V}{\partial \phi} = 0. \quad (18)$$

These equations, for static solutions, have one first integral given by  $F(X) - 2XF_X - V = D$ , where the integration constant  $D$  turns out to be the pressure  $p = D$ . We shall only deal with BPS states [21], which implies the condition  $p = 0$ . Moreover, this condition is also necessary for stability under Derrick's scaling, as shown in Ref.[3]. As the pressureless of the source makes the constant  $D$  to vanish the first integral for our problem is given by

$$F(X) - 2XF_X = V. \quad (19)$$

In the next section we shall use the “projection” method underlined in section II to construct two families of k-field models,  $A$  and  $B$ . The family  $A$  has two models,  $A1$  and  $A2$ , whose soliton solutions are analytically obtained as projections of the “angle”  $\bar{\phi}_0/a$  along the imaginary/real axis, respectively, with  $a$  an integer positive number which is precisely the power of the non-canonical kinetic term, i.e.  $X^a$ . Family  $B$  has also two models,  $B1$  and  $B2$  whose solutions are also obtained as projections but now of the “angle”  $\phi_0/a$  along the imaginary/real axis.

#### IV. FAMILY A OF K-FIELD MODELS

This section is divided into two parts depending on the value of  $a$  which is taken. In the first one we take  $a = 2$  to illustrate the general procedure while in the second one we extend the former results and take  $a > 2$ .

##### A. Family A of k-field models with $X^2$

Let us consider two models: the model  $L$  and the model  $W$  which support lump-like and wall soliton solutions respectively, as shown below, and whose lagrangians are given by

$$L_L = X|X| - \frac{3}{4} \sin^4(\bar{\phi}_0/2) \cos^4(\bar{\phi}_0), \quad (20)$$

and

$$L_W = X|X| - \frac{3}{4} \cos^4(\bar{\phi}_0/2) \cos^4(\bar{\phi}_0), \quad (21)$$

The first model, (20), admits the analytical solution

$$\phi_L(x) = 2 \cos \left[ \frac{\bar{\phi}_0(x)}{2} \right], \quad (22)$$

where  $\bar{\phi}_0$  is given in Eq.(12). This is a lump-like solution,

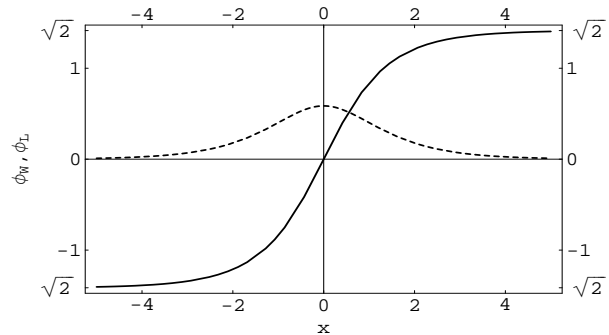


FIG. 1: Profile of the lump-like solution (dashed line) of model (20) and the wall (solid) of model (21) versus the distance  $x$ . The soliton is located at  $x = 0$ .

whose profile is shown in figure 1 (dashed line). The energy density associated to this field is given by  $\varepsilon = 4X^2 = \frac{4}{3}V$  (see figure 2) where the last equality is a simple consequence of Eq.(19). Note that the lump-like solution (22) can be seen as a “projection” over the real axis of the “angle”  $\bar{\phi}_0/2$ .

The second model, (21), admits the analytical solution

$$\phi_W(x) = 2 \sin \left[ \frac{\bar{\phi}_0(x)}{2} \right]. \quad (23)$$

Note that the field that we have constructed in (23) is a wall type one (see figure 1) with a topological charge  $Q = \frac{1}{2\sqrt{2}} \int_{-\infty}^{+\infty} \phi'_W(x) dx$ , and whose energy density is displayed in figure 2 (solid line).

We now note that the two models, (20) and (21), can be merged into a single one whose lagrangian density is simply given by

$$L = X|X| - \frac{3}{4} \left( 1 - \frac{\phi^2}{4} \right)^2 \left( -1 + \frac{\phi^2}{2} \right)^4. \quad (24)$$

Its equations of motion for BPS states, given by (18), are obtained as

$$-3X|X| = V \rightarrow \phi'^4 = \left( 1 - \frac{\phi^2}{4} \right)^2 \left( -1 + \frac{\phi^2}{2} \right)^4. \quad (25)$$

To see that the potential in Eq.(24) effectively gives the solution  $\phi_W$ , starting from (23) one can write  $X =$

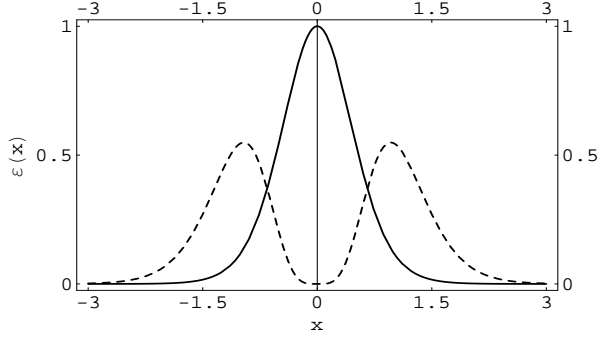


FIG. 2: Energy density versus the distance  $x$  for the wall solution (23) (solid line) and the lump-like solution (22) (dashed). The lump density has been increased by a factor of 100 in order to be plotted in the same figure as the wall one.

$-\frac{1}{2}\phi_W'^2(x) = -\frac{1}{2}\cos^2[\bar{\phi}_0/2]\cos^2[\bar{\phi}_0]$  and by transforming the cos terms into sin ones through trigonometric relations, and rewriting the final expression in terms of the field (23) one arrives to  $X = -\frac{1}{2}\left[\left(1 - \frac{\phi^2}{2}\right)^2\left(1 - \frac{\phi^2}{4}\right)\right]$ , and to the associated potential  $V(\phi) = -3X|X| = \frac{3}{4}\left[\left(1 - \frac{\phi^2}{2}\right)^4\left(1 - \frac{\phi^2}{4}\right)^2\right]$ , which is precisely the one of (24). A similar reasoning can be applied to the field  $\phi_L$  of Eq.(22), ending up in the lagrangian density (24) as well.

### B. Family A of k-field models with $X^a$ where $a > 2$

The previous model is a particular case of a more general family of models defined by lagrangian densities

$$L_L = X|X|^{a-1} - \frac{(2a-1)}{2^a}\sin^{2a}(\bar{\phi}_0/a)\cos^{2a}(\bar{\phi}_0), \quad (26)$$

and

$$L_W = X|X|^{a-1} - \frac{(2a-1)}{2^a}\cos^{2a}(\bar{\phi}_0/a)\cos^{2a}(\bar{\phi}_0), \quad (27)$$

which admit respectively the solutions

$$\phi_L(x) = a \cos\left[\frac{\bar{\phi}_0(x)}{a}\right]; \phi_W(x) = a \sin\left[\frac{\bar{\phi}_0(x)}{a}\right], \quad (28)$$

where we keep the notation  $L$  and  $W$  of the previous section. Note that the positivity of the energy (17) imposes the condition  $a > 1/2$  in the models above. Moreover the hyperbolicity condition for perturbations [24]

$$\frac{2XF_{XX} + F_X}{F_X} > 0, \quad (29)$$

is satisfied for  $a > 1/2$  which means that for the case considered here small perturbations over the background do not grow exponentially in time, ensuring the stability of the solutions.

### 1. Properties of the potentials $V_L$ and $V_W$

We now proceed further by studying the properties of the potentials  $V_L$  and  $V_W$  in order to argue the existence of soliton solutions.

First we note that when  $a = 1$  the solutions in (28) and the potentials in (26),(27) reduce to those of the standard lump and Klein-Gordon kink, respectively.

On the other hand for  $a = 2$  these potentials turn out to be the same and moreover equal to the one in (24) and thus we recover the above solutions (22) and (23), as expected. For greater values of  $a$ , one gets that when  $a$  is odd the potentials  $V_L$  and  $V_W$  are different (as we already saw for the particular case  $a = 1$ ), while for  $a$  even they coincide when written in terms of the fields  $\phi_L, \phi_W$ . For example, for  $a = 4$  we get

$$V_L = V_W = \frac{7}{16}\left[1 - \left(\frac{\phi_{L,W}}{4}\right)^2\right]^4\left[-1 + 2\left(1 - 2\left(\frac{\phi_{L,W}}{4}\right)^2\right)^2\right]^8. \quad (30)$$

Also, for both potentials, as  $a$  increases the number of vacua also increases, adding more topological sectors. In order to see the evolution on the number of these sectors with  $a$ , let us carefully analyze the vacua structure of these potentials.

$V_W$  is always positive and its zeroes are given by

$$\bar{Z}_n = a \sin\left[\left(n - \frac{1}{2}\right)\frac{\pi}{a}\right], \quad (31)$$

where  $n \in \mathbb{N}$ . The count of different zeros runs from  $n = 1$  to  $n = a/2 + 1$  ( $a$  even) or to  $n = (a + 1)/2$  ( $a$  odd). Explicitly the results are

$$\{\bar{Z}_1 = a, \bar{Z}_2, \dots, \bar{Z}_{\frac{a}{2}+1}, -\bar{Z}_{\frac{a}{2}+1}, \dots, -\bar{Z}_2, -\bar{Z}_1 = -a\}, \quad (32)$$

for  $a$  even and

$$\{\bar{Z}_1 = a, \bar{Z}_2, \dots, \bar{Z}_{\frac{a+1}{2}}, -\bar{Z}_{\frac{a+1}{2}}, \dots, -\bar{Z}_2, -\bar{Z}_1 = -a\}, \quad (33)$$

for  $a$  odd. The structure of zeroes is therefore symmetric in both cases.

Concerning the potential  $V_L$ , its zeroes are given by

$$\bar{Z}'_n = a \cos\left[\left(n - \frac{1}{2}\right)\frac{\pi}{a}\right], \quad (34)$$

and, explicitly, for  $a$  even the zeroes are obtained as

$$\{\bar{Z}'_1 = a, \bar{Z}'_2, \dots, \bar{Z}'_{\frac{a}{2}+1}, -\bar{Z}'_{\frac{a}{2}+1}, \dots, -\bar{Z}'_2, -\bar{Z}'_1 = -a\}, \quad (35)$$

while for  $a$  odd we have

$$\{a, \overline{Z}'_1, \overline{Z}'_2, \dots, \overline{Z}'_{\frac{a-1}{2}}, \overline{Z}'_{\frac{a+1}{2}} = 0, -\overline{Z}'_{\frac{a-1}{2}}, \dots, -\overline{Z}'_2, -\overline{Z}'_1, -a\}, \quad (36)$$

The potential  $V_L$  is always positive when  $a$  is even while for  $a$  odd it becomes negative beyond the farther zero ( $\pm a$ ) of the potential and moreover there is an additional central vacuum as compared with the other potentials. The height of the local maximums in between each pair of vacua decreases with  $a$  for both  $V_L$  and  $V_W$ . In figure 3 we have plotted this kind of behaviour for  $a$  odd ( $a = 3$ ) for both  $V_L$  and  $V_W$ , as an illustrative example of these families of potentials. For  $a$  even these potentials are equal, as already stated, and with a similar behaviour as the one for walls of  $a$  odd (solid line in Fig.3).

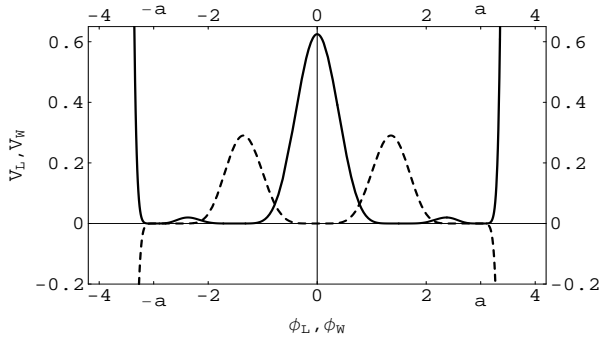


FIG. 3: The potentials  $V_W$  versus  $\phi_W$  (solid line) and  $V_L$  versus  $\phi_L$  (dashed) given in (26) and (27) for the case  $a = 3$ .

## 2. Evolution of $\phi_W$ and $\phi_L$ with $a$

Let us now analyze the evolution of the soliton solutions  $\phi_W$  and  $\phi_L$  with the parameter  $a$ . We will illustrate it by making use of some plots combined with the analysis of the topological charge.

We begin with  $\phi_W$ . In figure 4 we plot its evolution when  $a$  increases. As  $a = 1$  it gives the Klein-Gordon kink ( $a = 1$ ), with boundary conditions  $\phi(\pm\infty) = \pm 1$ . As  $a$  increases the height of the wall increases and in the limit of large  $a$  this family  $A$  of solutions approaches the cosine-Gordon soliton,  $\overline{\phi}_0$ , given in Eq.(12), with boundary values  $\overline{\phi}_0(\pm\infty) = \pm\pi/2$ . This can be easily seen by looking at the evolution of the topological charge: by introducing a topological current as

$$J_W^\mu = \frac{1}{2} \epsilon^{\mu\nu} \partial_\nu \phi_W, \quad (37)$$

we get for this case the (non-normalized) topological

charge

$$\begin{aligned} Q_W &= \int_{-\infty}^{+\infty} dx J_W^0 = \frac{1}{2} [\phi_W(+\infty) - \phi_W(-\infty)] \\ &= \frac{a}{2} (\sin[\overline{\phi}_0(+\infty)/a] - \sin[\overline{\phi}_0(-\infty)/a]) = \\ &= a \sin \left[ \frac{\pi}{2a} \right], \end{aligned} \quad (38)$$

which in particular gives  $Q_W(a = 1) = 1$  and  $Q_W(a \rightarrow$

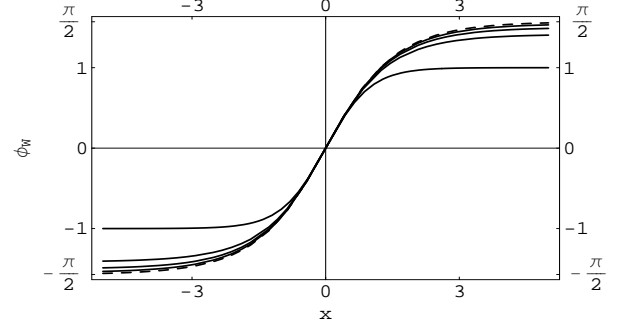


FIG. 4: Evolution with  $a$  ( $= 1, 2, 3, 4, 5$ ) of the wall profile,  $\phi_W$  versus the distance  $x$  for the family of models (27). The dashed line corresponds to the cosine-Gordon field profile,  $\overline{\phi}_0(x)$ , to which  $\phi_W$  converges in the large  $a$  limit. All the solitons are located at  $x = 0$ .

$\infty) \rightarrow \pi/2$ , thus connecting through a monotonic function of  $a$  the Klein-Gordon kink and the cosine-Gordon field. The non-vanishing of this topological charge indicates the presence of field configurations with a non-trivial topology, and whose presence guarantees the existence and stability of the wall.

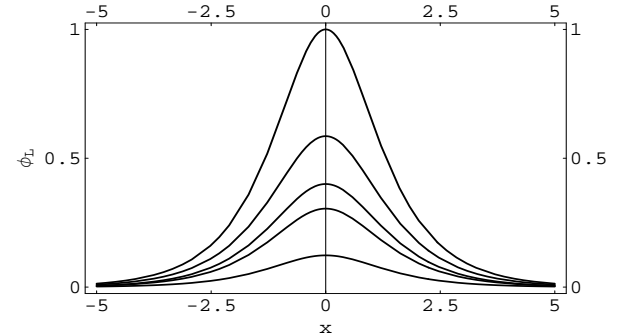


FIG. 5: From top to bottom, evolution with  $a$  ( $= 1, 2, 3, 4, 10$ ) of the lump profile,  $\phi_L$ , versus the distance  $x$  for the family of models (26). All the solutions are located at  $x = 0$  by applying appropriate shifts.

We now analyze the evolution of  $\phi_L$ . From Fig.5 we see that the height of the lump decreases as  $a$  increases as compared with the case  $a = 1$  (for which  $\phi_L(x = 0) = 1$ ), becoming more spread in space and disappearing in the limit of  $a \rightarrow \infty$ . Calculating the topological charge

associated to any of these solutions as in the previous case one gets

$$\begin{aligned} Q_L &= \frac{1}{2}[\phi_L(+\infty) - \phi_L(-\infty)] \\ &= \frac{a}{2}(\cos[\bar{\phi}_0(+\infty)/a] - \cos[\bar{\phi}_0(-\infty)/a]) \end{aligned} \quad (39)$$

which is identically zero for any value of  $a$ , as expected.

### 3. The energy density

The energy density associated to models (26)-(27) is obtained as

$$\begin{aligned} \varepsilon_W(a) &= -F(X) + V_W(\phi) = -2XF_X = -2aX|X|^{a-1} = \\ &= \frac{2a}{2a-1}V_W = \frac{2a}{2a} \cos^{2a}[\bar{\phi}_0/a] \cos^{2a}[\bar{\phi}_0] \end{aligned} \quad (40)$$

$$\begin{aligned} \varepsilon_L(a) &= -F(X) + V_L(\phi) = -2XF_X = -2aX|X|^{a-1} = \\ &= \frac{2a}{2a-1}V_L = \frac{2a}{2a} \sin^{2a}[\bar{\phi}_0/a] \cos^{2a}[\bar{\phi}_0] \end{aligned} \quad (41)$$

for walls and lumps, respectively. Its evolution with  $a$  for the case of walls is shown in figure 6, where we see that the energy density becomes more localized as we increase  $a$ .

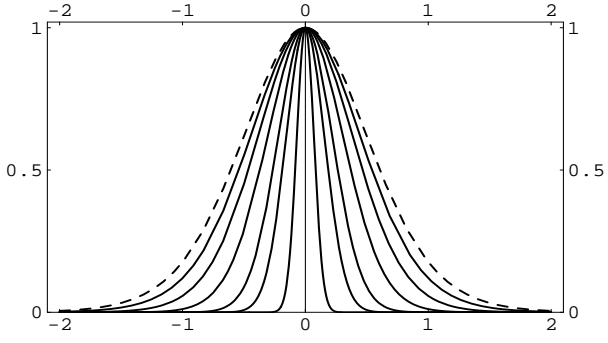


FIG. 6: From the exterior (dashed curve) to the interior, evolution of the factor  $\cos^{2a}[\bar{\phi}_0/a] \cos^{2a}[\bar{\phi}_0]$  in Eq.(40) with  $a$  ( $= 2, 3, 5, 10, 20, 100$ ) for the wall solution and versus the distance  $x$ . All the solitons are located at  $x = 0$ . The dashed line corresponds to the canonical kinetic term case ( $a = 1$ ).

### C. Family B of k-field models with $X^a$

Let us consider now another family of models with lagrangian densities

$$L_1 = X|X|^{a-1} - \frac{(2a-1)}{2a} \sin^{2a}[\phi_0/a] \sin^{2a}[\phi_0], \quad (42)$$

and

$$L_2 = X|X|^{a-1} - \frac{(2a-1)}{2a} \cos^{2a}[\phi_0/a] \sin^{2a}[\phi_0], \quad (43)$$

which admit analytical solutions constructed as projections over the real and imaginary axes of the solutions of the sine-Gordon system given in Eq.(6), i.e.

$$\phi_1(x) = -a \cos \left[ \frac{\phi_0(x)}{a} \right]; \phi_2(x) = a \sin \left[ \frac{\phi_0(x)}{a} \right]. \quad (44)$$

#### 1. Properties of the potentials $V_1$ and $V_2$

From the expressions above it follows that both potentials coincide when  $a$  is even, and differ when  $a$  is odd, as for the family A. For example, for the case  $a = 2$ , expanding the above expressions we get

$$V_1(a=2) = V_2(a=2) = \frac{3}{4} \left( 1 - \frac{\phi_{1,2}^2}{4} \right)^4 \phi_{1,2}^4, \quad (45)$$

which shows their equal analytical expression in terms of the fields  $\phi_1$  and  $\phi_2$ . Note that in this potential the point  $\phi_1 = 0$  is now a minimum, instead of a maximum, as opposed to the previous family of models. Again this is a general result for  $a$  even: in this case there are  $(\frac{a}{2})$  symmetric vacua and an additional central vacuum for both potentials, which are always positive. For  $a$  odd there are  $(\frac{a+1}{2})$  symmetric vacua for both  $V_1$  and  $V_2$ . However, there is now an additional central vacuum for  $V_2$ , and this potential becomes negative beyond the farther vacuum, while  $V_1$  is always positive and reaches a maximum at the center. In all cases the height of each successive maximum of the potential decreases as we move away from  $\phi = 0$ . The zeroes are obtained, for  $V_1$ , as

$$Z_n = a \cos \left[ n \frac{\pi}{a} \right], \quad (46)$$

and are given, explicitly, by

$$\{Z_1 = a, Z_2, \dots, Z_{\frac{a}{2}}, Z_{\frac{a}{2}+1} = 0, -Z_{\frac{a}{2}}, \dots, -Z_2, -Z_1 = -a\}, \quad (47)$$

for  $a$  even and

$$\{Z_1 = a, Z_2, \dots, Z_{\frac{a+1}{2}}, -Z_{\frac{a+1}{2}}, \dots, -Z_2, -Z_1 = -a\}, \quad (48)$$

for  $a$  odd. And for  $V_2$  the zeroes

$$Z'_n = a \sin \left[ n \frac{\pi}{a} \right], \quad (49)$$

are obtained as

$$\{Z'_1 = a, Z'_2, \dots, Z'_{\frac{a}{2}}, Z'_{\frac{a}{2}+1} = 0, -Z'_{\frac{a}{2}}, \dots, -Z_2, -Z_1 = -a\}, \quad (50)$$

for  $a$  even and

$$\{a, Z'_1, Z'_2, \dots, Z'_{\frac{a-1}{2}}, Z'_{\frac{a+1}{2}} = 0, -Z'_{\frac{a-1}{2}}, \dots, -Z'_2, -Z'_1 = -a\}. \quad (51)$$

for  $a$  odd. Note that in the case  $a = 1$  we recover, for  $V_1$ , the Mexican hat potential of the  $\phi^4$ -model while for  $V_2$  we recover the potential of the standard lump, a similar situation as for the potentials  $V_W$  and  $V_L$  of the previous family  $A$ . This is indeed a general conclusion for  $a$  odd: the potentials  $V_1$  and  $V_2$  coincide, as functions of their arguments, with  $V_W$  and  $V_L$ , respectively. The typical behaviour of  $V_1$  and  $V_2$  in this case is similar as for the first family ( $A$ ) and figure 3 above is again illustrative of this generic behaviour. This is not so when  $a$  is even as the potential has now a minimum at  $\phi = 0$  and it is positive everywhere, thus resembling neither  $V_W$  nor  $V_L$ .

## 2. Evolution of $\phi_1$ and $\phi_2$ with $a$

For  $a = 1$   $\phi_1$  describes the Klein-Gordon kink while  $\phi_2$  corresponds to the standard lump potential, as expected from the analysis of the potentials in this case. This is in agreement with the fact that through a  $\pi/2$  rotation between the imaginary and real axis one changes the boundary conditions of the soliton solutions in such a way that the topological wall solution may be changed into a non-topological lump-like one and viceversa. Now, as we increase  $a$  we can follow the evolution of  $\phi_1$ , which leads to wall-like solutions which become thicker with  $a$  until they disappear in the limit  $a \rightarrow \infty$ . This can be seen through the evolution of the (non-normalized) topological charge, written as

$$\begin{aligned} Q_1(a) &= \int_{-\infty}^{+\infty} \phi'_1(x) dx = \frac{a}{2} [\phi_1(+\infty) - \phi_1(-\infty)] = \\ &= -\frac{a}{2} (\cos[\phi_0(+\infty)/a] - \cos[\phi_0(-\infty)/a]) \quad (52) \\ &= \frac{a}{2} \left[ 1 - \cos \left[ \frac{\pi}{a} \right] \right] \end{aligned}$$

which gives  $Q_1(a = 1) = 1 = Q_{KG}$  and  $Q_1(a \rightarrow \infty) \rightarrow 0$ , as expected. Now if we look at the evolution of  $\phi_2$  with  $a$ , it can be shown that its non-normalized charge is given by

$$Q_2(a) = \frac{a}{2} (\sin[\phi(+\infty)/a] - \sin[\phi(-\infty)/a]) = \frac{a}{2} \sin \left[ \frac{\pi}{a} \right] \quad (53)$$

which vanishes for  $a = 1$ , as is expected for the lump, but for  $a = 2$  takes the value  $Q_2 = 2$ , undergoing a topology change from a lump-like solution to a wall one.

This evolution can be followed through figure 7, where the soliton profile is plotted. There the solution begins being a lump-like, transforms into a wall and in the limit  $a \rightarrow \infty$  the family of solutions approaches to the sine-Gordon kink since  $Q(a \rightarrow \infty) \rightarrow \pi = Q_{SG}$  when both charges are non-normalized.

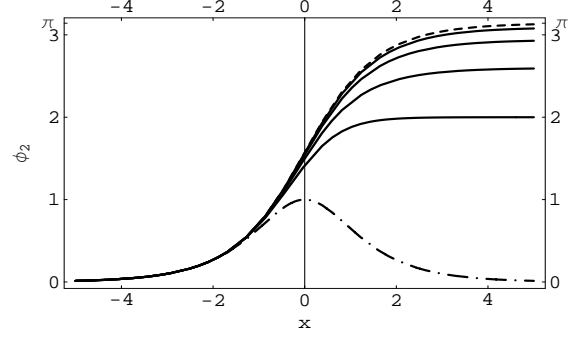


FIG. 7: Soliton profile of  $\phi_2$  versus the distance  $x$  for different values of (from bottom to top)  $a = 2, 3, 5, 10$  (solid lines) connecting the standard lump solution ( $a = 1$ , dashed-dotted line) with the sine-Gordon kink ( $a \rightarrow \infty$ , dashed line).

## 3. The energy density

The energy density for this family of solutions is given by

$$\varepsilon_1(a) = \frac{2a}{2^a} \sin^{2a}[\phi_0/a] \sin^{2a}[\phi_0] \quad (54)$$

$$\varepsilon_2(a) = \frac{2a}{2^a} \cos^{2a}[\phi_0/a] \sin^{2a}[\phi_0]. \quad (55)$$

The evolution of  $\varepsilon_2(a)$  as we increase  $a$  is shown (apart from the factor  $2a/2^a$ ) in Fig. 8, where we see the change of profile from the lump ( $a = 1$ ) to the wall ( $a \geq 2$ ) and how the energy density becomes more localized as we increase  $a$ .  $\varepsilon_1(a)$  fades out with  $a$ , vanishing in the large  $a$  limit.

## D. Generalizations of families A and B

For each of the families of models considered before we can define a more general one including at the same time  $V_W$  and  $V_L$  for the first family and  $V_1$  and  $V_2$  for the second one. To do this we include a constant  $C$  into the wall solution  $\phi_W$  of the family  $A$  as

$$\bar{\phi} = a \sin \left[ \frac{\bar{\phi}_0}{a} + C \right], \quad (56)$$

in such a way that for  $C = 0$  we recover the wall solution of (28) while for  $C = \pi/2$  we obtain the lump-like one of

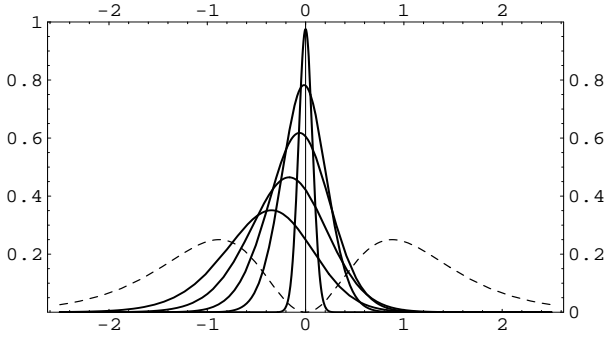


FIG. 8: Behaviour with the distance  $x$  of the factor  $\cos^{2a}[\phi_0/a] \sin^{2a}[\phi_0]$  of  $\varepsilon_2(q)$  in Eq.(55) as (from bottom to top)  $a$  evolves ( $= 2, 3, 5, 10, 100$  solid lines), starting from the canonical kinetic term case ( $a = 1$ , dashed line). Note the change in the shape of the energy density in the transition from the lump-like solution ( $a = 1$ ) to the first wall one ( $a = 2$ ).

(28). This is indeed a simple rotation of  $\pi/2$  of the sin over the cos transforming a wall into a lump. Moreover we can write  $C = m\pi$  so for  $m$  integer the field (56) describes (anti-)walls, while for  $m$  semi-integer it describes lumps. Now there is a single potential containing both families, which is obtained as

$$\bar{V}(\bar{\phi}) = \frac{2a-1}{2a} \cos^{2a}[\arcsin[\bar{\phi}/a]] \cos^{2a}[a(\arcsin[\bar{\phi}/a] + C)]. \quad (57)$$

The same procedure can be applied to the second family ( $B$ ), obtaining in this case a single field

$$\phi = -a \cos \left[ \frac{\phi_0}{a} + C' \right], \quad (58)$$

which gives  $\phi_1$  of Eq.(44) for  $C' = 0$  and  $\phi_2$  for  $C' = \pi/2$ , transforming one solution into the other through a rotation of  $\pi/2$ , as in the former case. The associated single potential is

$$V(\phi) = \frac{2a-1}{2a} \sin^{2a}[\arccos[-\phi/a]] \cdot \sin^{2a}[a(\arccos[-\phi/a] + C')]. \quad (59)$$

Note that in both cases, aside from the cases  $C = C' = 0$  and  $C = C' = \pi/2$ , which give the solutions already studied, we have now new solutions for other values of  $C$ , which can be interpreted as composed states of kinks/anti-kinks, possibly interacting between themselves, and whose analysis is beyond the aim of this paper.

## V. PROJECTION AND DEFORMATION METHODS

In this section we compare our results with those obtained using a generalization of the deformation method for k-fields.

Let  $\varphi$  be generically the cosine/sine-Gordon fields and  $V$  the respective potential. Its equation of motion is simply

$$\varphi' = (2V(\varphi))^{\frac{1}{2}}, \quad (60)$$

Now let  $\chi$  be generically the fields for the k-models  $A$  and  $B$ , and  $U$  the respective potential. Its equation of motion is

$$\chi' = \left( \frac{2^a}{2a-1} U(\chi) \right)^{\frac{1}{2a}}. \quad (61)$$

We shall now apply the deformation method (see Ref. [6]) between the sine/cosine-Gordon models and the k-field families, in both directions.

### A. Deforming the k-field models $A$ and $B$ into the canonical cosine-Gordon and sine-Gordon models

Let us first look for the deformation function that deforms the k-field models  $A/B$  into the canonical cosine/sine-Gordon models, respectively. Thus  $\varphi$  will be seen as the deformed field. We also take the deformation function as  $f(\varphi)$ . Therefore

$$\chi = f(\varphi). \quad (62)$$

Using Eqs.(60)-(61) we get that

$$\frac{df}{d\varphi} = \frac{1}{\sqrt{2}} \left( \frac{2^a}{2a-1} U(\chi \rightarrow \varphi) \right)^{\frac{1}{2a}} \frac{1}{V(\chi)^{\frac{1}{2}}}. \quad (63)$$

Making some simple calculations one can obtain the deformation functions associated to the four models defined by the families  $A/B$  considered before. They are given by

$$\begin{aligned} f_L^A(\varphi) &= a \cos(\varphi/a) \\ f_W^A(\varphi) &= a \sin(\varphi/a) \\ f_1^B(\varphi) &= -a \cos(\varphi/a) \\ f_2^B(\varphi) &= a \sin(\varphi/a), \end{aligned} \quad (64)$$

which exactly reproduce the projection functions given in Eqs.(28) and (44). Through these functions it can be seen that via Eq.(63) the potentials of the cosine-Gordon (9) and sine-Gordon (2) are obtained from the k-field potentials in Eqs.(26) and (27) for model A and in Eqs.(42) and (43) for model B, respectively. Therefore we conclude that the canonical cosine/sine-Gordon models can be seen as deformations of the k-field models  $A/B$ , respectively. Note that this procedure transforms a given k-field model (i.e.  $a$  fixed) with a finite number of topological sectors, into the periodic (infinite) structure of vacua of the cosine/sine-Gordon system.



## B. Deforming the canonical cosine/sine-Gordon models into the k-field models $A$ and $B$

We now apply the deformation method in the opposite way. Thus  $\chi$  will be seen as the deformed field. We now take the deformation function as  $g(\chi)$  with

$$\frac{dg}{d\chi} = \frac{1}{\frac{d\varphi}{d\chi}} \quad (65)$$

and one obtains, explicitly

$$\begin{aligned} g_L^A(\chi) &= a \arccos(\chi/a) \\ g_W^A(\chi) &= a \arcsin(\chi/a) \\ g_1^B(\chi) &= a \arccos(-\chi/a) \\ g_2^B(\chi) &= a \arcsin(\chi/a), \end{aligned} \quad (66)$$

which can be shown to transform the cosine/sine-Gordon potentials into the four k-field potentials of models  $A/B$  via the deformed potential

$$U(\chi) = \frac{2a-1}{2^{a-1}} \frac{V(\varphi \rightarrow g(\chi))^a}{\left(\frac{dg}{d\chi}\right)^{2a}}. \quad (67)$$

Therefore, as expected, we can also conclude that the canonical cosine/sine-Gordon models can be deformed into the k-field models  $A/B$ , respectively.

## VI. CONCLUSIONS

In this paper we have presented a projection method allowing to obtain analytical soliton solutions of wall or lump-like type for k-field theories defined as powers of the standard canonical kinetic term. We have used the sine-Gordon soliton and its cosine-Gordon counterpart, as a system of utmost physical and mathematical interest, in order to illustrate this procedure. The solutions of these k-field models reduce to the standard Klein-Gordon kink and the standard lump in the lowest case ( $a = 1$ ) of the projection while some of them approach to the cosine/sine-Gordon models in the limit  $a \rightarrow \infty$ . During the evolution with  $a$  the topology of the solution may change, transforming a lump into a wall or the opposite.

We have shown that this method can be seen as a generalization of the deformation method for k-fields of the form  $X^a$ . Using this we concluded that the models that we presented, i.e.,  $A/B$  can be seen as deformed models of the canonical cosine/sine-Gordon, respectively, and viceversa. This fact opens the possibility of extending the deformation method to k-field theories with more general non-canonical kinetic terms. This issue deserves a separate analysis, a task to be carried out in a future work.

## Acknowledgments

D. R.-G. is partially funded by the Centro de Física

do Porto, and would like to thank the Departamento de Física e Astronomia da Faculdade de Ciências da Universidade do Porto for all their hospitality while doing this work. C. dS. is partially funded under the FCT project CERN/FP/116358/2010. The authors would like to thank F. Pacetti for useful discussions.

## Appendix A: Spatially localized and modulated solutions

In this annex we present a slight modification of model (43). We define a new lagrangian

$$L_B = X|X|^{a-1} - \frac{(2a-1)}{2^a} \cos^{2a}[b\bar{\phi}_0] \cos^{2a}[\bar{\phi}_0], \quad (A1)$$

where  $b$  is a free parameter for a given model. In par-

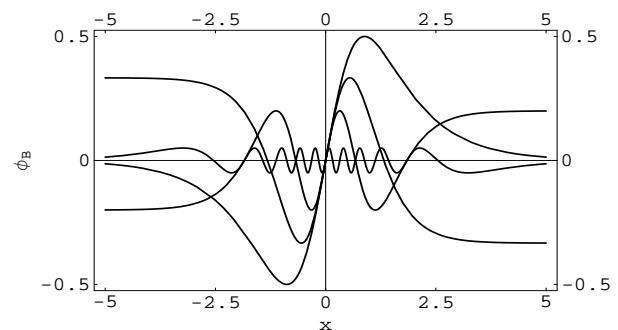


FIG. 9:  $\phi_B$  profile in Eq.(A2) versus the distance  $x$  for models (A3) for values  $b = 2, 3, 5, 10$  and  $a = 2$ , showing the different possible kinds of asymptotic behaviours. Note that the height of the maxima decreases with  $b$ .

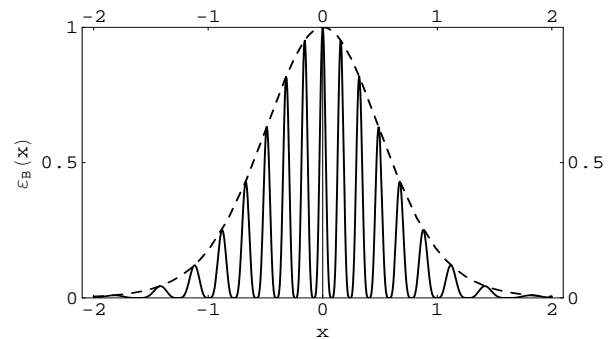


FIG. 10:  $\epsilon_B$  in Eq.(A3) in the case  $a = 2$  and  $b = 20$ , with the dashed line representing the envelope  $\cos^4[\bar{\phi}_0]$ .

ticular, for the case  $b = 1/a$  the above model coincides with the one in Eq.(27), and its associated solutions with those of (28). We shall however consider in this annex the case of  $b > 1$ , which describes non-linear solutions which are spatially localized and modulated. The scalar field and the energy density are given by

$$\phi_B = \frac{1}{b} \sin[b \cdot \bar{\phi}_0] \quad (\text{A2})$$

$$\varepsilon_B = \frac{2a}{2a} \cos^{2a}[b\bar{\phi}_0] \cos^{2a}[\bar{\phi}_0]. \quad (\text{A3})$$

Note that the profile of this solution does not depend on the power of the kinetic term, but just on the parameter  $b$ . In figure 9 we have plotted  $\phi_B(x)$  for several values of  $b$ . We see that as  $b$  increases the solution shows

more peaks while its height decreases. Moreover several distinct behaviours are found as we make  $b$  to evolve. Concerning the energy density in Eq.(A3), it describes damped oscillations in space, with an envelope given by  $\cos^{2a}[\bar{\phi}_0]$ , as can be seen in figure 10 for the particular case of  $a = 2$  and  $b = 20$ .

We believe that this kind of configurations has possible applications in the context of breather solutions, which shall be investigated elsewhere.

- 
- [1] T. H. R. Skyrme, Proc. R. Soc. Lond. A **260**, 127 (1961); S. Deser, M. J. Duff, C. J. Isham, Nucl. Phys. B **114**, 29 (1976); N. Manton, P. Sutcliffe, in *Topological solitons* (Cambridge, Cambridge/UK, 2004).
- [2] E. Babichev, Phys. Rev. D **74**, 085004 (2006); E. Babichev, Phys. Rev. D **77**, 065021 (2008).
- [3] D. Bazeia, L. Losano, R. Menezes, J. C. R. E. Oliveira, Eur. Phys. J. C **51**, 953 (2007).
- [4] J. Garriga, V. F. Mukhanov, Phys. Lett. B **458**, 219 (1999); C. Armendariz-Picon, T. Damour, V. F. Mukhanov, Phys. Lett. B **458**, 209 (1999); C. Armendariz-Picon, V. F. Mukhanov, P. J. Steinhardt, Phys. Rev. Lett. **85**, 4438 (2000); T. Chiba, T. Okabe, M. Yamaguchi, Phys. Rev. D **62**, 023511 (2000); C. Armendariz-Picon, V. F. Mukhanov, P. J. Steinhardt, Phys. Rev. D **63**, 103510 (2001).
- [5] C. Adam, J. Sanchez-Guillen, A. Wereszczynski, J. Phys. A **40**, 13625 (2007); Erratum-ibid. A **42**, 089801 (2009); C. Adam, P. Klimas, J. Sanchez-Guillen, A. Wereszczynski, J. Phys. A **42**, 135401 (2009); D. Bazeia, E. da Hora, R. Menezes, H. P. de Oliveira, C. dos Santos, Phys. Rev. D **81**, 125016 (2010); C. dos Santos, Phys. Rev. D **82**, 125009 (2010).
- [6] D. Bazeia, L. Losano, J. M. C. Malbouisson, Phys. Rev. D **66**, 101701(R) (2002).
- [7] J. Rubinstein, J. Math. Phys. **11**, 258 (1970); M. J. Ablowitz, D. J. Kaup, A. C. Newell, H. Segul, Phys. Rev. Lett. **30**, 1262 (1973); L. D. Faddeev, L. A. Takhtajan, V. E. Zakharov, Sov. Phys. Dokl. **19**, 824 (1975); J. Hruby, Nucl. Phys. B **131**, 275 (1977); S. Ferrara, L. Girardello, S. Sciuto, Phys. Lett. B **76**, 303 (1978).
- [8] M. A. Lohe, Phys. Rev. D **20**, 3120 (1979).
- [9] D. Bazeia, L. Losano, J. M. C. Malbouisson, J. R. L. Santos, *Preprint arXiv:1104.0376 [hep-th]*; D. Bazeia, M. A. Gonzalez Leon, L. Losano, J. Mateos Guilarte, Phys. Rev. D **73**, 105008 (2006); D. Bazeia, L. Losano, J. M. C. Malbouisson, Physica D **237**, 937 (2008); D. Bazeia, L. Losano, R. Menezes, M. A. M. Souza, Eur. Phys. Lett. **87**, 21001 (2009).
- [10] A. C. Scott, *Nonlinear Science* (Oxford University Press, Oxford, 1999).
- [11] G. L. Lamb, Jr., *Elements of Soliton Theory* (Wiley-Interscience, New York, 1980).
- [12] L. P. Eisenhart, *A Treatise on the Differential Geometry of Curves and Surfaces* (Dover, New York, 1980).
- [13] O. Babelon, D. Bernard, M. Talon, in *Introduction to Classical Integrable Systems* (Cambridge University Press, Cambridge, U.K., 2003); L. D. Faddeev, in *Integrable Models in 1 + 1 Dimensional Quantum Field Theory*, Proceedings of the Les Houches Summer School of Theoretical Physics, 1982 (Elsevier Science, Amsterdam, 1984); L. D. Faddeev, L. A. Takhtajan, in *Hamiltonian Methods in the Theory of Solitons* (Springer, Berlin, 1986).
- [14] M. Cvetič, H. H. Soleng, Phys. Rep. **282**, 159 (1997).
- [15] P. Brax, C. van de Bruck, A. -C. Davis, Rep. Prog. Phys. **67**, 2183 (2004).
- [16] M. L. Manseld, R. H. Boyd, J. Polym. Sci. Phys. Ed. **16**, 1227 (1978); J. L. Skinner, P. G. Wolynes, J. Chem. Phys. **73**, 4015 (1980); F. Zhang, M. A. Collins, Chem. Phys. Lett. **214**, 459 (1993); D. Bazeia, E. Ventura, Chem. Phys. Lett. **303**, 341 (1999); E. Ventura, A. M. Simas, D. Bazeia, Chem. Phys. Lett. **320**, 587 (2000); D. Bazeia, V. B. P. Leite, B. H. B. Lima, F. Moraes, Chem. Phys. Lett. **340**, 205 (2001); J. Belmonte-Beitia, V. M. Perez-Garcia, V. Vekslerchik, V. V. Konotop, Phys. Rev. Lett. **100**, 164102 (2008).
- [17] Z. Bryant, et al., Nature **424**, 338 (2003); M. Peyrard, Nonlinearity **17**, R1 (2004).
- [18] M. Hassaine, C. Martinez, Class. Quant. Grav. **25**, 195023 (2008); H. A. Gonzalez, M. Hassaine, C. Martinez, Phys. Rev. D **80**, 104008 (2009).
- [19] D. Bazeia, A. R. Gomes, L. Losano, R. Menezes, Phys. Lett. B **671**, 402 (2009).
- [20] A. Vilenkin, E. P. S. Shellard, in *Cosmic strings and other topological defects* (Cambridge, Cambridge/UK, 1994); P. P. Avelino, C. J. A. P. Martins, J. Menezes, R. Menezes, J. C. R. E. Oliveira, Phys. Rev. D **73**, 123519 (2006); P. P. Avelino, C. J. A. P. Martins, J. Menezes, R. Menezes, J. C. R. E. Oliveira, Phys. Rev. D **73**, 123520 (2006).
- [21] M. K. Prasad, C. M. Sommerfeld, Phys. Rev. Lett. **35**, 760 (1975); E. B. Bogomolnyi, Sov. J. Nucl. Phys. **24**, 449 (1976).
- [22] M. J. Ablowitz, P. A. Clarkson, in *Solitons, Nonlinear Evolution Equations and Inverse Scattering* (Cambridge University Press, Cambridge, U.K., 1999).
- [23] L. A. Ferreira, B. Piette, W. J. Zakrzewski, Phys. Rev. E **77**, 036613 (2008).
- [24] C. Armendariz-Picon, E. A. Lim, JCAP **0508**, 007 (2005); A. D. Rendall, Class. Quant. Grav. **23**, 1557 (2006).